THE JOURNAL OF BIOLOGICAL CHEMISTRY VOL. 289, NO. 35, pp. 24588–24598, August 29, 2014

Structural and Spectroscopic Insights into BolA-Glutaredoxin Complexes[S]

Received for publication, April 10, 2014, and in revised form, July 10, 2014 Published, JBC Papers in Press, July 10, 2014, DOI 10.1074/jbc.M114.572701

Thomas Roret[‡§], Pascale Tsan[‡§], Jérémy Couturier[¶‖1], Bo Zhang[**], Michael K. Johnson[**], Nicolas Rouhier[¶‖1], and Claude Didierjean[‡§2]

From the [‡]Université de Lorraine and [§]CNRS, UMR 7036 CRM2, BioMod group, 54506 Vandœuvre-lès-Nancy, France, [¶]Université de Lorraine, UMR 1136 Interactions Arbres Microorganismes, F-54500 Vandœuvre-lès-Nancy, France, [‖]INRA, UMR 1136 Interactions Arbres Microorganismes, F-54280 Champenoux, France, and [**]Department of Chemistry and Center for Metalloenzyme Studies, University of Georgia, Athens, Georgia 30602

Background: BolA and glutaredoxin interact together in the iron metabolism.
Results: They form two types of heterodimers with different binding surfaces depending on the presence or absence of an iron-sulfur cluster.
Conclusion: The function of both proteins is likely modulated by the nature of the interaction.
Significance: Understanding the molecular mechanisms responsible for iron sensing is crucial for all iron-mediated cellular processes.

BolA proteins are defined as stress-responsive transcriptional regulators, but they also participate in iron metabolism. Although they can form [2Fe-2S]-containing complexes with monothiol glutaredoxins (Grx), structural details are lacking. Three *Arabidopsis thaliana* BolA structures were solved. They differ primarily by the size of a loop referred to as the variable [H/C] loop, which contains an important cysteine (BolA_C group) or histidine (BolA_H group) residue. From three-dimensional modeling and spectroscopic analyses of *A. thaliana* GrxS14-BolA1 holo-heterodimer (BolA_H), we provide evidence for the coordination of a Rieske-type [2Fe-2S] cluster. For BolA_C members, the cysteine could replace the histidine as a ligand. NMR interaction experiments using apoproteins indicate that a completely different heterodimer was formed involving the nucleic acid binding site of BolA and the C-terminal tail of Grx. The possible biological importance of these complexes is discussed considering the physiological functions previously assigned to BolA and to Grx-BolA or Grx-Grx complexes.

Because proteins usually function in macromolecular complexes, identifying protein-protein interactions constitute an essential step toward the understanding of protein networks and functions. The description of these interactions is difficult because they can for example be very transient, or a given protein can have multiple partners involving different or overlapping binding sites, or more rarely it can have a single partner but different modes of interactions (1). BolAs were initially defined as stress-responsive transcriptional regulators whose overexpression in *Escherichia coli* modified bacterial shape and induced biofilm formation (2, 3), whereas glutaredoxins (Grxs)[3] were long thought to uniquely function as glutathione (GSH)-dependent oxidoreductases (4). It was thus surprising that a BolA, referred to as Fra2 (Fe repressor of activation-2), and cytosolic monothiol Grx3/4 contributed to the regulation of iron homeostasis by forming stable [2Fe-2S] cluster-bridged holo-heterodimers controlling the nuclear translocation of the *Saccharomyces cerevisiae* Aft1/Aft2 transcription factors in response to a mitochondrial signal (5–7). Hence, BolA may modify monothiol Grx functions by converting Grx homodimers bridging a labile [2Fe-2S] cluster into a heterodimer containing a more stable [2Fe-2S] cluster (7). This cluster is ligated by two cysteines (one from Grx and one from a GSH molecule) and one histidine (invariant histidine of BolAs), but the fourth ligand is unknown (7, 8). On the other hand, it was reported that Grx-BolA couples from various sources could also form apo-heterodimers (7, 9). This is consistent with the observation that an *in vivo* Grx3/4-Fra2 interaction is found both in iron-replete and iron-depleted yeast cells (5).

However, none of these Grx-BolA complexes was structurally characterized at the atomic scale. In *Arabidopsis thaliana* there are three genes encoding BolA proteins (AtBolA1, AtBolA2, and AtBolA4). In addition, the sulfurtransferase AtSufE1 contains a C-terminal BolA domain (^{SufE1}BolA) that is only present in plant members (10). From a previously established classification, these AtBolAs can be separated into two groups that contain either a conserved histidine (AtBolA1, AtBolA4, and ^{SufE1}BolA; BolA_H group) or cysteine (AtBolA2;

[S] This article contains supplemental Figs. S1–S3.
The resonance assignments and relaxation data of AtBolA2 and the NMR chemical shift mapping of AtGrxS14-BolA2 are available at the Biological Magnetic Resonance Data Bank (codes 19849 and 19850).
The atomic coordinates and structure factors (codes 2MM9, 2MMA, 4PUG, and 4PUI) have been deposited in the Protein Data Bank (http://wwpdb.org/).

[1] Supported by a grant overseen by ANR (Grant 2010BLAN1616) as part of the "Investissements d'Avenir" program (ANR-11-LABX-0002-01, Lab of Excellence ARBRE).

[2] To whom correspondence should be addressed: Université de Lorraine, UMR7036 CRM2, BioMod group, 54506 Vandœuvre-lès-Nancy, France. Tel.: 33-383684879; E-mail: claude.didierjean@univ-lorraine.fr.

[3] The abbreviations used are: Grx, glutaredoxins; AtGrx, *A. thaliana* glutaredoxin; ^{SufE1}BolA, C-terminal BolA domain of the sulfurtransferase SufE1; [H/C] loop, loop containing the histidine and cysteine residues from BolA_H and BolA_C groups; ScGrx, *S. cerevisiae* glutaredoxin; HSQC, heteronuclear single quantum correlation; r.m.s.d., root mean square deviation; KH, K-homology; HTH, helix-turn-helix.

BolA_C group) residue (11). Besides solving the structure of AtBolAs by x-ray crystallography or NMR spectroscopy, apo- and holo-heterodimers formed between AtBolAs and monothiol AtGrxs have been characterized using three-dimensional modeling, UV-visible absorption/CD, EPR, and resonance Raman and NMR spectroscopies. The results indicated the formation of two types of complexes involving distinct regions of both partners and facilitated identification of the ligands for [2Fe-2S] cluster-bridged heterodimers involving for the first time a BolA_H member.

EXPERIMENTAL PROCEDURES

Plasmid Constructions—The cloning of AtBolA1 (At1g55805), AtBolA2 (At5g09830), BolA domain of AtSufE1 (At4g26500), AtGrxS14 (At3g54900), and AtGrxS17 (At4g04950) into pET vectors was described previously (10, 12). For AtBolA1, another version coding a protein deprived of the first 63 amino acids instead of 51 amino acids was cloned into pET12a using 5′-CCCCCCCCCATATGGCAATAGAGAA-TCGA-3′ (AtBolA1_for) and 5′-CCCGGATCCCTAGTCTT-TAGAAGGAGA-3′ (AtBolA1_rev) primers to shorten the unstructured N-terminal part that likely prevented its crystallization. For co-expression experiments, the sequences coding for an N-terminally His-tagged AtGrxS14 and an untagged AtBolA1 were inserted into the first and second cloning sites (NcoI/BamHI and NdeI/XhoI) of a pCDFDuet plasmid by subcloning His_6-AtGrxS14 from pET15b and by amplifying AtBolA1 from a pET12a::AtBolA1 using 5′-CCCCCCCCCAT-ATGAGCAGCGTTGAGAAAACC-3′ (AtBolA1_for2) and 5′-CCCCCTCGAGCTAGTCTTTAGAAGG-3′ (AtBolA1_rev2) primers and subsequent insertion into the second cloning site.

Expression and Purification of Recombinant Proteins—Unlabeled tagged or untagged proteins were expressed and purified as previously (10, 12). For simple ^{15}N (AtGrxS14) or double ^{15}N- and ^{13}C-labeled proteins (AtBolA2), cells were grown in M9 minimal medium supplemented with $^{15}NH_4Cl$ (1 g/liter) and either D-glucose or D-[^{13}C]glucose (2 g/liter). For protein co-expression, an *E. coli* BL21(DE3) colony transformed by pCDFDuet HisAtGrxS14-BolA1 was grown at 37 °C in LB media. The culture was induced with 1 mM isopropyl 1-thio-β-D-galactopyranoside at $A_{600} = 0.45$, and the bacterial cultures were further cultivated at 34 °C for 5 h. The cells were collected by centrifugation at 5000 × *g* for 15 min at 4 °C and stored at −80 °C. 7 g of cell paste were thawed and resuspended in 50 mM Tris-HCl buffer at pH 7.8 containing 1 mM GSH, 10 μg/ml phenylmethylsulfonyl fluoride, 15 μg/ml DNase, and 5 μg/ml RNase. The cells were lysed by sonication, and cell debris was removed by centrifugation at 39,700 g for 1 h at 4 °C. The following chromatographic purification processes were carried out inside a glove box ($O_2 < 2$ ppm) with degassed buffers. The extract was loaded onto a 2 × 5-ml His-Trap column (GE Healthcare) equilibrated with binding buffer (50 mM Tris-HCl, pH 7.8, containing 1 mM GSH, 0.5 M NaCl, and 20 mM imidazole). The column was washed with 5 column volumes of binding buffer before elution with a linear gradient of 20 to 500 mM imidazole. The purest fractions containing AtGrxS14 and AtBolA1 were concentrated using an YM10 Amicon ultrafiltration. Anaerobic reconstitution experiments were carried out by incubating AtGrxS14-BolA1 with a 10-fold excess of ferrous ammonium sulfate and L-cysteine and catalytic amounts of IscS in the presence of 5 mM GSH. The reconstitution reaction was carried out under strictly anaerobic conditions (<2 ppm O_2) at room temperature for 1.5 h. Excess reagents were then removed by a HiTrap Q-Sepharose, and fractions containing Fe-S cluster-bound proteins were concentrated by ultrafiltration. Protein concentrations were determined using BSA as a standard (Roche Applied Science) with Bio-Rad Dc protein assay in conjunction with the microscale-modified procedure (13). Iron concentrations were determined after $KMnO_4$/HCl protein digestion (14) using a 1000 ppm atomic absorption iron standard to prepare standard solutions of known iron concentration (Fluka). All sample concentrations and ε or Δε values are expressed based on the concentration of the AtGrxS14-BolA1 complex.

UV-Visible Absorption/CD, Resonance Raman and EPR Measurements—All samples for spectroscopic investigations were prepared under an argon atmosphere in the glove box unless otherwise noted. UV-visible absorption and CD spectra were recorded in sealed anaerobic 1-mm quartz cuvettes at room temperature using a Shimadzu UV-3101 scanning spectrophotometer and a Jasco J-715 spectropolarimeter, respectively. Resonance Raman spectra were recorded at 22 K on frozen droplets of sample mounted on the cold finger of a Displex Model CSA-202E closed cycle refrigerator (Air Products, Allentown, PA) using a Ramanor U1000 scanning spectrometer (Instruments SA, Edison, NJ) coupled with a Sabre argon-ion laser (Coherent, Santa Clara, CA). X-band (~9.6 GHz) EPR spectra were recorded using a ESP-300D spectrometer (Bruker, Billerica, MA) equipped with an ER-4116 dual mode cavity and an ESR 900 flow cryostat (Oxford Instruments, Concord, MA). Spin quantification were assessed by double integration with reference to a 1 mM Cu (EDTA) samples using non-power saturating conditions for both sample and standard.

Crystallization, Data Collection, Structure Determination, and Refinement—AtBolA1 and ^{SufE1}BolA were crystallized by the microbatch under oil method at 278 K. 2 μl of AtBolA1 (8.25 mg/ml) were crystallized by mixing with 2.1 μl of crystallization solution containing a mixture of 18% PEG4000, 6% 2-propanol, 6% 2.5 hexanediol, 4% xylitol, and 0.07 M sodium acetate. 2 μl of ^{SufE1}BolA (8.60 mg/ml) were crystallized by mixing with 1.6 μl of crystallization solution containing a mixture of 12% PEG20000, 6% ethylene glycol, 0.02 M trimethylamine HCl, and 0.1 M MES, pH 6.5. They were flash-cooled in liquid nitrogen after a short soak in crystallization solution premixed with 20% glycerol as a cryoprotectant. X-ray diffraction experiments were performed at 100 K at beamline FIP-BM30A (European Synchrotron Radiation Facility, Grenoble, France) for AtBolA1 and at beamline PROXIMA 1 (SOLEIL, Saint-Aubin, France) for ^{SufE1}BolA. Their data sets at 2.0 and 1.7Å, respectively, were indexed and processed using XDS (15) and scaled and merged with Scala (16) from the CCP4 program package (17). Both structures were solved by molecular replacement with Molrep (18) using the *Mus musculus* BolA1 coordinates (PDB entry 1V60) as first search model. Structures were refined using automatic calculations from PHENIX (19) with manual inspection and corrections using Coot (20) (Table 1).

TABLE 1
Crystallographic statistics

	AtBolA1	^{SufE1}BolA
Data collection		
Beam line	FIP-BM30A	PROXIMA 1
Space group	$C222_1$	$C2$
Unit cell (Å)	30.09, 179.88, 66.82	95.83, 31.63, 68.63
Resolution (Å)	45.0–2.0	46.2–1.7
Unique reflections	12,798/1,790	20,575/2,902
Average redundancy	4.6/4.5	3.2/2.6
Completeness (%)	99.8/98.9	99.5/97.2
R_{merge}	0.10/0.35	0.03/0.36
I/σ	11.3/4.1	20.6/2.6
Refinement		
Resolution (Å)	45.0-2.0	46.2-1.7
R_{free}/R	22.58/19.94	21.32/19.13
Total number of atoms	1,659	1,533
Water	206	165
Average B factor	24.11	32.95
r.m.s.d.		
Bonds	0.003	0.006
Angles	0.849	1.066
MolProbity analysis		
Clashscore, all atoms	3.09 (99%)	1.46 (99%)
MolProbity score	1.10 (100%)	0.88 (100%)

TABLE 2
Statistics from NMR structure calculations of AtBolA2 using ARIA2 and CNS
VDW, van der Waals; ELEC, electrostatic; Cdih violations, CNS structure calculation output logs for dihedral angle restraint violations.

Experimental restraints	
Total NOEs	2248
Intraresidue	504
Sequential	789
Medium	624
Long range	331
Restraints statistics	
r.m.s.d. from standard geometry	
Bond (Å)	0.0057 ± 0.0004
Angle (°)	0.72 ± 0.03
Improper (°)	2.05 ± 0.20
Dihedral (°)	40.31 ± 0.19
Energies of final structures (kcal.mol^{-1})	
E_{TOTAL}	−3368.76 ± 106.42
E_{bond}	48.69 ± 6.30
E_{angle}	211.10 ± 19.54
$E_{improper}$	468.16 ± 94.15
$E_{dihedral}$	496.48 ± 4.58
E_{VDW}	−845.88 ± 8.01
E_{ELEC}	−3,747.30 ± 78.36
r.m.s.d. backbone, residue 1–80 (Å)	0.56 ± 0.12
r.m.s.d. backbone, all (Å)	0.89 ± 0.61
NOE violations >0.5 Å	0.75 ± 0.91
Cdih violations >5°	3.25 ± 1.29

The validation of the crystal structures was performed with MolProbity (21). The atomic coordinates for AtBolA1 (PDB entry 4PUG) and ^{SufE1}BolA crystal (PDB entry 4PUI) structures are available at the Research Collaboratory for Structural Bioinformatics (RCSB) Protein Data Bank.

NMR Analyses—The AtBolA2 NMR samples typically contained 0.9 mM uniformly ^{15}N or ^{13}C,^{15}N-labeled protein in 50 mM phosphate, pH 6.0, 10% (v/v) D_2O and 0.02% (w/v) sodium azide under nitrogen atmosphere. All NMR experiments were carried out at 298 K on a Bruker spectrometer (600 MHz) equipped with a cryogenic probe. NMR data were processed with NMRPipe (22) and analyzed with NMRViewJ (23). ^{1}H, ^{13}C, and ^{15}N assignment was obtained from ^{1}H,^{15}N HSQC, ^{1}H,^{15}N TOCSY (two-dimensional total correlation spectroscopy)-HSQC (mixing time Tm = 80 ms), ^{1}H,^{15}N NOESY-HSQC (Tm = 100 ms and 150 ms), HNHA, HNHB, HNCA, HNCO, HN(CA)CO, and CBCA(CO)NH spectra. Aromatic side chains signals were assigned using COSY, TOCSY, and NOESY homonuclear experiments in D_2O. 2248 distance restraints were derived from NOESY experiments. 150 ψ dihedral restraints were obtained by DANGLE program (24) or from $^3J_{HNH\alpha}$ in CcpNmr (25). 59 hydrogen bond restraints were inferred from slowly exchanging amide protons identified on a ^{1}H, ^{15}N HSQC recorded after redissolving lyophilized protein in D_2O. These restraints were applied in an iterative structure calculation and a simulated annealing protocol with water refinement at the end using ARIA2.3 (26) and CNS1.21 (27) (Table 2). 100 structures were generated, and the 20 structures of lowest energy were kept. The backbone root mean square deviation (r.m.s.d.) among the 20 lowest-energy structures is 0.89 Å for the whole protein. Structural quality was analyzed using MolProbity (21). ^{15}N relaxation parameters were determined using NMRViewJ (23) from ^{15}N R_1 (relaxation delays: 2, 50, 100, 200, 400, 600, 900, and 1200 ms), R_2 (15.68, 31.36, 47.04, 62.72, 78.40, 94.08, 125.44, and 156.80 ms), and ^{1}H,^{15}N heteronuclear NOE experiments. Interaction experiments were carried at pH 7.0. ^{1}H,^{15}N HSQC were typically recorded with 0.12 mM uniformly ^{15}N-labeled AtBolA2 (or AtGrxS14) samples. 0.1, 0.2, 0.5, 1, and 2 eq of unlabeled AtGrxS14/GrxS17 (or AtBolA2/BolA1) were successively added using a 0.4 mM stock sample. The apo-heterodimer AtGrxS14-BolA2 structure was obtained by docking using GRAMM-X Protein-Protein Docking Web Server v.1.2.0 (28) coupled to an energy refinement using YAMBER force field from YASARA (29). Residues exhibiting either chemical shift variations above 2 S.D. or large signal broadening were defined as interface residues in the docking protocol. The atomic coordinates for AtBolA2 NMR structures (PDB entry 2MM9) and the AtGrxS14-BolA2 apo-heterodimer model (2MMA) are available at the Research Collaboratory for Structural Bioinformatics (RCSB) Protein Data Bank.

Intrinsic Fluorescence Properties of AtGrxS14—Fluorescence was recorded with a Cary Eclipse spectrofluorometer (Agilent) with 1-cm path length cuvettes. Prior to measurement, 10 μM AtGrxS14 in Tris-HCl 30 mM pH 8.0 buffer was incubated or not with varying concentrations of AtBolA1 ranging from 5 to 30 μM at 25 °C for 10 min. The resulting fluorescence was recorded between 280 and 450 nm after excitation at 270 nm. For determining the apparent K_d value, the decrease in AtGrxS14 fluorescence at 337 nm was plotted against AtBolA1 concentration using the one binding site hyperbola model (GraphPad Prism 6 software) and the following equation: fluorescence intensity = B_{max} * [AtBolA1]/(K_d + [AtBolA1]), where B_{max} represents the fluorescence intensity of maximal binding.

Sequence Analyses—All proteins of the BolA/YrbA family and all proteins that contain a BolA domain, *i.e.* around 12,000 sequences from Uniprot database, have been retrieved. After removing identical sequences but also transit peptides and protein regions that do not strictly belong to a BolA domain, 2444 sequences were aligned using MAFFT (31). As a starting point, a structural alignment was performed by Strap (32) using the 11 known BolA structures. This structural alignment is used in MAFFT (31) with the 2444 sequences to make a final alignment.

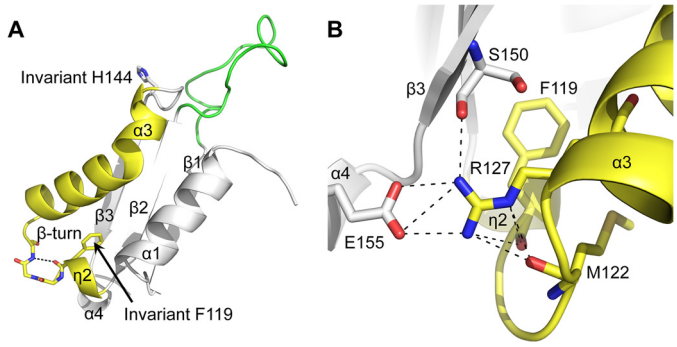

FIGURE 1. **BolA overall fold.** *A*, the Phe-119 and His-144 invariant residues and the β-turn are plotted on the x-ray structure of AtBolA1. The potential nucleic acid binding region containing the HTH structural motif is in *yellow*, and the [H/C] loop containing the putative [2Fe-2S] cluster ligands is in *green*. *B*, putative hydrogen bonds involving Arg-127 in AtBolA1.

RESULTS AND DISCUSSION

AtBolA Structures Support the Existence of Two Different Groups—Two BolA categories were previously distinguished from primary structure analyses: those having a conserved cysteine (Cys-29 in AtBolA2; BolA_C group) and those having another conserved histidine (His-109 and His-324 in AtBolA1 and ^{SufE1}BolA, respectively; BolA_H group) in addition to an invariant histidine. Crystallization of the chloroplastic BolA1 and of the C-terminal domain of SufE1 (^{SufE1}BolA) from *A. thaliana* provided two BolA_H structures, solved at high resolution (2.0 and 1.7 Å, respectively). The solution structure of the nucleocytoplasmic AtBolA2, which belongs to the BolA_C group, was obtained by NMR using standard heteronuclear experiments. All these structures revealed a well conserved fold, although a structure-based sequence alignment of ~2500 non-redundant BolA sequences revealed only two invariant residues, Phe-119 and His-144 (AtBolA1 numbering). This structural alignment has been used thereafter to determine residue conservation.

Solved AtBolA models exhibit an α/β-structure made of four helices and three strands with an α1β1β2η2α3β3α4 (η: 3_{10}-helix) topology (Fig. 1*A*) that is similar to previously described BolA models (33). All β-strands (7–8 residues) form a central three-stranded β-sheet scaffold (β1 anti-parallel to β2 and β3) with the α4 helix anchored at one side of the β-sheet, whereas other helices are on the opposite side. A local structural difference can, however, be noticed in the solution structure of AtBolA2. According to the NMR data, especially to the D_2O exchange experiments, β3 is split into two short strands, β3′ and β3″, connected by an additional Lys-71 residue, an insertion found mostly in plant BolA_C (84% *versus* 2% in other kingdoms). The BolA invariant phenylalanine is located in η2 (Fig. 1*A*) and seems essential for BolA unique hydrophobic core, whereas the invariant histidine is found at the N-terminal end of β3.

All secondary structures are connected by short loops (1–4 residues) except the one situated between β1 and β2. This β1-β2 loop that we refer to as [H/C] loop contains the histidine and cysteine residues from BolA_H and BolA_C groups, respectively. In accordance with the existence of two groups, the [H/C] loop can be formed by 11 ± 6 (up to 20) residues in BolA_H members, whereas it is generally only 7 ± 2 residues in BolA_C members. In BolA_H, the histidine (His-109 in AtBolA1), located before the N-terminal end of β2, is in most cases followed by an aromatic amino acid (Tyr/Phe in 87% of BolA_H). In BolA_C, the cysteine (Cys-29 in AtBolA2) is frequently surrounded by glycines in a GGCG signature (69%) and is usually located three residues before the histidine position found in BolA_H.

An Arginine of the Conserved Face Governs α4-Helix Formation—The most conserved residues in BolAs including the histidine or cysteine of the [H/C] loop, the invariant histidine and phenylalanine are generally found in the same region termed the "conserved face" by Kasai *et al.* (33). From all AtBolA structures, it seems also that the side chain of an arginine residue (Arg-127 in AtBolA1) present in α3-helix is involved in tertiary structure maintenance (Fig. 1*B*). This arginine corresponds to the first arginine of a well conserved "RHR" signature (present in 41% of the sequences). It may be replaced by a glutamine in some proteins, but in plant BolAs it is mostly invariant (97%). Several putative intramolecular hydrogen bonds exist between its guanidinium group and four residues located in distinct protein regions, *i.e.* with carbonyl group of Phe-119 (in η2), Met-122 (in η2-α3 loop), and Ser-150 (in β3) and with Glu-155 carboxylate group (in α4) (Fig. 1*B*). This last interaction probably governs α4-helix formation because it is the sole polar link between α4 and the rest of the protein. Accordingly, in *Ehrlichia chaffeensis* and *Rickettsia prowazekii* BolA structures (PDB entry 2KZ0 and 2MCQ, respectively), two examples where the arginine residue is replaced by a glutamine, the C-terminal end is shorter by seven residues, and α4 is missing.

The Helix-turn-helix (HTH) Motif of BolAs Is Potentially Involved in DNA Binding—Currently, only bacterial BolA_H members have been shown to act as transcriptional regulators by binding to gene promoters (34, 35), whereas Uvi31+, a BolA_H from *Chlamydomonas reinhardtii,* likely exhibits endonuclease activity (36). The capacity to bind nucleic acids is in line with the fact that BolA possesses an overall fold related to the one found in type II K-homology (KH) domain-containing proteins (33) known to bind nucleic acids.

In KH domains the nucleic acid binding region involves the third β-strand and a HTH structural motif, formed by the two consecutive helices of the KH motif αββαααβ with a short connecting G*XX*G loop (type II β-turn) (37). The interaction of KH domains with nucleic acids is stabilized by electrostatic interactions, with a positively charged patch on the HTH structural motif interacting with the negatively charged phosphate/sugar backbone of nucleic acids. The HTH motif in BolAs is different due to the absence of the G*XX*G loop between helices η2 and α3. In AtBolAs, this connection between η2 and α3 helices is an outgrowth of 4 residues *versus* 2 for canonical KH domains. This loop contains the invariant phenylalanine in a specific F*XG*X signature (type II β-turn). The glycine is also a well conserved residue (>90% conserved in all organisms). In plant BolAs the capacity to bind nucleic acids would arise mainly from a positively charged patch (RHR signature present in α3) that is part of the conserved face (Fig. 2*A*). It brings a strong positive charge around the protruding turn of the HTH motif, whereas the rest of the conserved face is nearly neutral and the

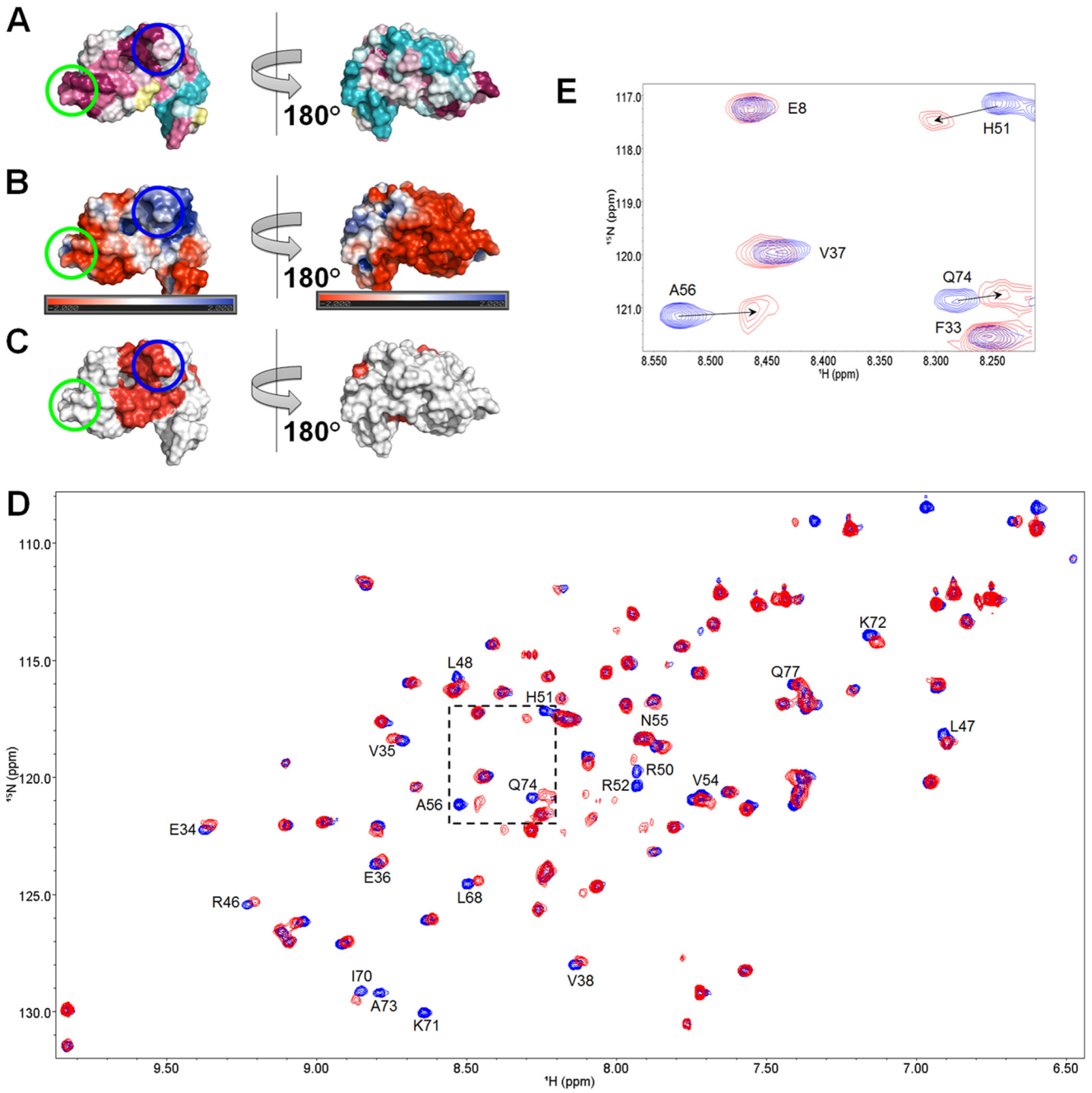

FIGURE 2. **Interaction of AtBolA2 with AtGrxS14.** *A*, the *left panel* displays the conserved face of BolAs, and the *right panel* displays the variable face of BolAs. Residue conservation ranges from 0% (*cyan*) to 100% (*purple*). RHR signature (*blue circle*) and putative ligands of the [2Fe-2S] cluster (*green circle*) are also highlighted on AtBolA2 surface. *B*, electrostatic potential of AtBolA2 generated by APBS (57) and showing negative charges in *red* and positive charges in *blue*. *C*, mapping of the residues of AtBolA2 (*red*) involved in the interaction with AtGrxS14, as shown by NMR. *D*, overlay of ^{1}H,^{15}N HSQC spectrum of AtBolA2 (*blue*) and ^{1}H,^{15}N HSQC spectrum of AtGrxS14-BolA2 at a 1:1 ratio (*red*). The assigned peaks are indicated with the residue number and one- letter code. *E*, zoom of the area delimited by *dashed lines* in D. The *arrows* indicate the direction in which the amide peak shifts upon the addition of AtGrxS14.

"variable face" globally negative (Fig. 2*B*). Another difference is that, compared with their corresponding helices in KH domains, helices η2 and α3 do not have the same length. Despite this difference, the orientation of the second helix remains rather similar, which suggests that the predominant role of "DNA recognition helix" found in KH domains is conserved in BolAs. Finally, it is noticeable that a loop resembling the variable [H/C] loop present between the two consecutives β-strands in BolAs is also present in type II KH domains (37).

The HTH Motif of BolAs Is Involved in Glutaredoxin Recognition—Because BolAs have the ability to interact both with DNA and Grx apoforms, we sought to determine interaction surfaces (7, 10). The interaction was studied using NMR spectroscopy by performing chemical shift mapping on AtBolA2 with its biological partner AtGrxS17 but also with AtGrxS14, whose x-ray structure was solved (38). Upon the addition of unlabeled AtGrxS14, some peaks of AtBolA2 in the ^{1}H,^{15}N HSQC spectrum experience show significant chemical

shift perturbations and line broadening (Fig. 2, *D* and *E*). These peaks correspond to residues Glu-34–Glu-36, Val-38, Leu-47–Leu-48, Arg-50–Arg-52, Val-54–Ala-56, Leu-68, Lys-71–Gln-74, and Gln-77, which are located around the positively charged RHR signature of α3 (Fig. 2*C* and supplemental Fig. S1*A*), and thus coincides with the putative nucleic acid binding region. Interestingly, it does not include the BolA invariant histidine involved in the [2Fe-2S] cluster ligation (39). Although the quality of the resulting spectra was poorer due to the larger size of the complex, a similar interface was determined using AtGrxS17 (supplemental Fig. S1*B*). Overall, it indicates that the BolA interaction surface with Grxs and nucleic acids is similar, suggesting that the formation of Grx-BolA apo-heterodimer should modify the nucleic acid binding capacity of BolAs.

The C-terminal Region of Glutaredoxins Is Involved in BolA Recognition in Grx-BolA Apo-heterodimer—The residues in Grxs involved in the formation of Grx-BolA apo-heterodimers were mapped by NMR using AtGrxS14 in interaction with its biological partner AtBolA1 (a BolA_H) but also with AtBolA2 (a BolA_C, 17.5% identity with AtBolA1). The addition of unlabeled AtBolA1 or AtBolA2 induced similar perturbations on the $^{1}H,^{15}N$ HSQC spectrum of AtGrxS14 (supplemental Fig. S1, *C* and *D*), which was assigned from $^{1}H,^{15}N$ heteronuclear three-dimensional experiments. Residues identified as involved in the interaction are Val-79, Lys-83, Val-85, Gln-105, Leu-110, Val-112, Lys-130–Ser-133, Trp-135, Thr-137, Gln-140, Ile-143, Glu-146-Phe-148, Ile-153, Leu-155–Glu-166, and Glu-168. They are mainly located at the C terminus, forming a negatively charged patch around a quite conserved "GEL" motif present in the last α-helix and opposite to the CGFS active site (supplemental Fig. S2).

Although NMR is a very sensitive method, the relevance of these apoGrx-BolA interactions was further examined by measuring variations in the intrinsic fluorescence of AtGrxS14 in the presence of AtBolA1 since AtGrxS14 has a single Trp residue (Trp-135), which is part of the interaction area, and AtBolA1 has no Trp residue. As expected, adding increasing concentrations of AtBolA1 quenched AtGrxS14 fluorescence (Fig. 3*A*). From this experiment, a dissociation constant (K_d) of 7 ± 2 μM was determined for the AtBolA1-AtGrxS14 couple (Fig. 3*B*), suggesting that this interaction may be physiologically relevant.

Altogether, these data describing AtGrxS14-[BolA1/BolA2] interactions represent the first structural description of a complex between a monothiol Grx and a transcriptional regulator. Considering that the RHR signature in BolAs and the sequence surrounding the GEL motif in Grxs are mostly conserved, this type of interaction may be extended to all monothiol Grx and BolA couples. For instance, in plants there is at least one BolA and one monothiol Grx in subcellular compartments possessing DNA and/or an Fe-S cluster biosynthesis machinery (10). It is worth noting that the importance of the C-terminal region in Grxs for protein-protein interactions was already evident in the examples of Aft1 and TGA transcription factors (supplemental Fig. S2) (40, 41).

The [H/C] Loop Should Contain the Fourth Fe-S Cluster Ligand in Grx-BolA_C Holo-heterodimers—A remarkable property of BolAs is their capacity to form [2Fe-2S]-bridged

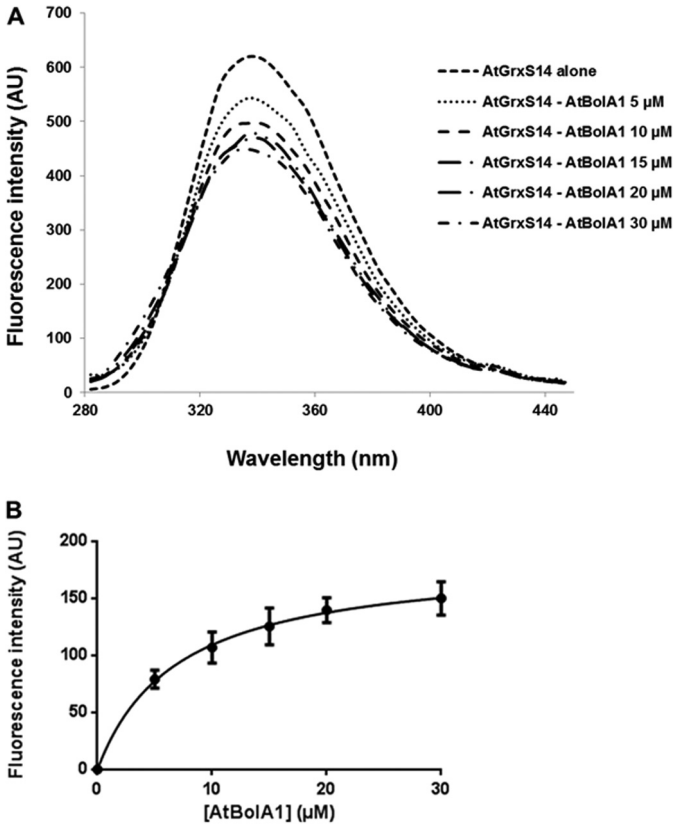

FIGURE 3. **Influence of AtBolA1 on AtGrxS14 intrinsic fluorescence.** *A*, representative experiment showing the changes in AtGrxS14 fluorescence in the presence of increasing concentrations of AtBolA1. *B*, decrease of fluorescence emission at 337 nm was plotted against AtBolA1 concentration to determine the K_d value using a hyperbola equation. The data are represented as mean ± S.D. of three separate experiments. *AU*, arbitrary units.

dimers with Grxs, but all ligands are not identified (39). From known BolA_C structures, the only conserved candidate residue of the [H/C] loop that has the ability to coordinate an iron atom and is spatially close to the invariant histidine is the cysteine of the GGCG motif. In available AtBolA2 model structures, this cysteine is clearly too far from the invariant histidine to serve as a cluster ligand with measured distances of 5 up to 15 Å. Hence, a conformational rearrangement of the [H/C] loop should occur to place this cysteine at an adequate position for serving as a [2Fe-2S] cluster ligand. The presence of a majority of small residues such as glycines could confer the necessary backbone flexibility for this loop. Supporting this view, relaxation data on AtBolA2 showed a slight decrease in the $^{1}H,^{15}N$ heteronuclear NOE values for this loop (supplemental Fig. S3), which indicates an increased mobility on fast (ps-ns) time scale and suggests that such a rearrangement is possible. What is more puzzling is that the mutation of the equivalent cysteine (Cys-66) in *S. cerevisiae* Fra2 neither abolishes Fe-S cluster formation into ScGrx3-Fra2 complex nor significantly changes its spectroscopic signature (8). However, although the mutagenesis work performed on all histidine and cysteine residues failed to identify the fourth ligand, the spectroscopic characterization of the ScGrx3-Fra2 heterodimer indicated that this residue could be another cysteine but not another histidine.

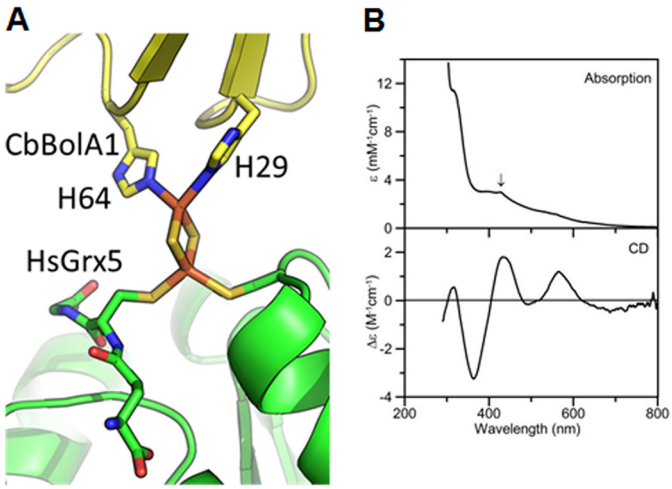

FIGURE 4. **Glutaredoxin-BolA_H holo-heterodimer.** *A*, model of the Grx-BolA holo-heterodimer with Rieske-type [2Fe-2S] coordination built using human Grx5 (PDB entry 2WUL) (58) and *C. burnetii* BolA, which coordinates a cobalt atom via His-29 and His-64 (PDB entry 3TR3). These residues are ideally positioned to coordinate an iron atom of a [2Fe-2S] cluster instead of cobalt, and they were used to orientate the BolA domain in the heterodimeric model. *B*, UV-visible absorption and CD spectra of AtGrxS14-BolA1 heterodimers. ϵ and $\Delta\epsilon$ values are expressed per AtGrxS14-BolA1 heterodimer, and the *arrow* indicates the Soret band from a trace heme impurity. *AU*, arbitrary units.

Rieske-type [2Fe-2S] Coordination Occurs in Grx-BolA_H Holo-heterodimers—In available BolA_H structures, the histidine from the [H/C] loop is close to the invariant histidine and could potentially serve as the unknown ligand. Moreover, contrary to Cys-66 in Fra2, its position is imposed by the presence of the β2 strand. Interestingly, in the x-ray structure of a *Coxiella burnetii* BolA_H, a cobalt atom is ligated by these two histidines, mimicking iron ligation. From this structure and that of a monothiol Grx homodimer, a model for a Grx-BolA holo-heterodimer with Rieske-type [2Fe-2S] coordination can be easily built (Fig. 4*A*). In this model, the distance required between the two nitrogen atoms to coordinate an iron atom should be around 3.5 Å, which can be reached via a simple change of histidine rotamer in AtBolA1 and ^{SufE1}BolA structures. To confirm this possibility, the plastidial *A. thaliana* GrxS14 and BolA1 were co-expressed in *E. coli*. Purification under anaerobic conditions resulted in a Grx-BolA complex with partial [2Fe-2S] cluster occupancy (~0.3 cluster per heterodimer) and a trace amount of heme impurity, as judged by iron and protein analysis, UV-visible, absorption, and CD absorption spectroscopies (Fig. 4*B*). Homogeneous samples containing 2.1 ± 0.2 iron/heterodimer and with ϵ_{400} values = 8.5 ± 0.2 $mM^{-1}cm^{-1}$, both indicative of one [2Fe-2S] cluster/heterodimer, were obtained by anaerobic reconstitution in the presence of 5 mM GSH and repurification on a Q-Sepharose column (Fig. 5*A*). The corresponding CD spectrum of the $[2Fe\text{-}2S]^{2+}$ cluster-bound AtGrxS14-BolA1 complex is significantly different from that of the [2Fe-2S] cluster-bridged AtGrxS14 homodimer (Fig. 5*B*). However, the CD spectrum is similar to that of the ScGrx3-Fra2 holo-heterodimer except that the pronounced positive bands at 440 and 565 nm in AtGrxS14-BolA1 shift to 425 and 583 nm, respectively, in ScGrx3-Fra2 (Fig. 5*B*). Resonance Raman spectra of $[2Fe\text{-}2S]^{2+}$ clusters are sensitive to ligand type and conformation and provided evidence for the presence of a single histidyl [2Fe-2S] cluster ligand in the ScGrx3-Fra2 heterodimer (7) and complete cysteinyl ligation for [2Fe-2S] clusters in ScGrx3 and AtGrxS14 homodimers (7, 12). A comparison of the resonance Raman spectra of the $[2Fe\text{-}2S]^{2+}$ centers in ScGrx3-Fra2 and AtGrxS14-BolA1 heterodimers and the AtGrxS14 homodimer is shown in Fig. 5*C*. Both heterodimer spectra show multiple bands in the low energy region (250–300 nm), which are indicative of histidyl ligation (7). Moreover, the observation of three bands in this region for AtGrxS14-BolA1 (250, 282, and 296 cm^{-1}) compared with two for ScGrx3-Fra2 (275 and 300 cm^{-1}) is tentatively interpreted as the former involving two rather than one histidyl ligand at the unique iron site. The 250-cm^{-1} band would have a major contribution from symmetric stretching of the two Fe-N (His) bonds, with one or both of the 282 and 296 cm^{-1} bands having a significant contribution from asymmetric stretching of the two Fe-N(His) bonds. The available pH dependence and N-isotope shift data for the Rieske-type and mitoNEET proteins argues against the assignment of the band in the 250–300 cm^{-1} region to pure Fe-N(His) stretching mode (42–45). Rather, Fe-N(His) stretching is distributed over low energy Fe-S stretching modes and internal modes of coordinated cysteine ligands and enhanced via the visible S-to-Fe charge transfer transitions.

The most definitive spectroscopic evidence for a Rieske-type ligation in AtGrxS14-BolA1 heterodimer comes from EPR studies of the dithionite-reduced complex (Fig. 5*D*). Whereas the $[2Fe\text{-}2S]^{2+}$ clusters in homodimeric Grxs are reductively labile, the $[2Fe\text{-}2S]^{2+}$ cluster in AtGrxS14-BolA1 is quantitatively reduced by dithionite to stable $[2Fe\text{-}2S]^{1+}$ centers, as observed in ScGrx3-Fra2 heterodimer (7, 12). For AtGrxS14-BolA1, this is illustrated by the UV-visible absorption/CD and EPR studies. The inset in Fig. 5*A* shows the anomalous near axial resonance (g = 2.02, 1.96, 1.65, g_{av} = 1.88) of the $[2Fe\text{-}2S]^{1+}$ center in dithionite-reduced AtGrxS14-BolA1, which accounts for 1.0 ± 0.1 spins per [2Fe-2S] cluster. The resonance is very different from that observed for the $[2Fe\text{-}2S]^{1+}$ center in dithionite-reduced ScGrx3-Fra2 (g = 2.01, 1.92, 1.87, g_{av} = 1.93) (Fig. 5*C*). The g value anisotropy and g_{av} value of $S = 1/2$ $[2Fe\text{-}2S]^{1+}$ centers are determined primarily by the distortion and ligation at the localized-valence Fe(II) site (46, 47). The g_{av} values are generally in the range 1.95–1.97 for complete cysteinyl ligation, 1.93–1.94 for 3 cysteinyl and 1 histidyl ligand, and 1.88–1.92 for Rieske-type centers with 2 cysteinyl ligands at the Fe(III) site and 2 histidyl ligands at the Fe(II) site (7, 48). Hence the g_{av} value puts the $[2Fe\text{-}2S]^{1+}$ center in AtGrxS14-BolA1 heterodimer firmly in the Rieske-type class. However, the g value isotropy is not typical of reduced Rieske proteins, which generally exhibit rhombic resonances. Thus the near axial resonance with $g_{\perp} > g_{\parallel}$ is anomalous for Rieske proteins but can be interpreted in terms of a distinct type of distortion involving an increased (His)N-Fe-N(His) angle that would result in a predominant d_{xx2-y2} ground state (46). In summary, the proposed holo-heterodimer model shows a domain arrangement totally different from the one found in the apo-heterodimer model derived from NMR data (Fig. 6*A*).

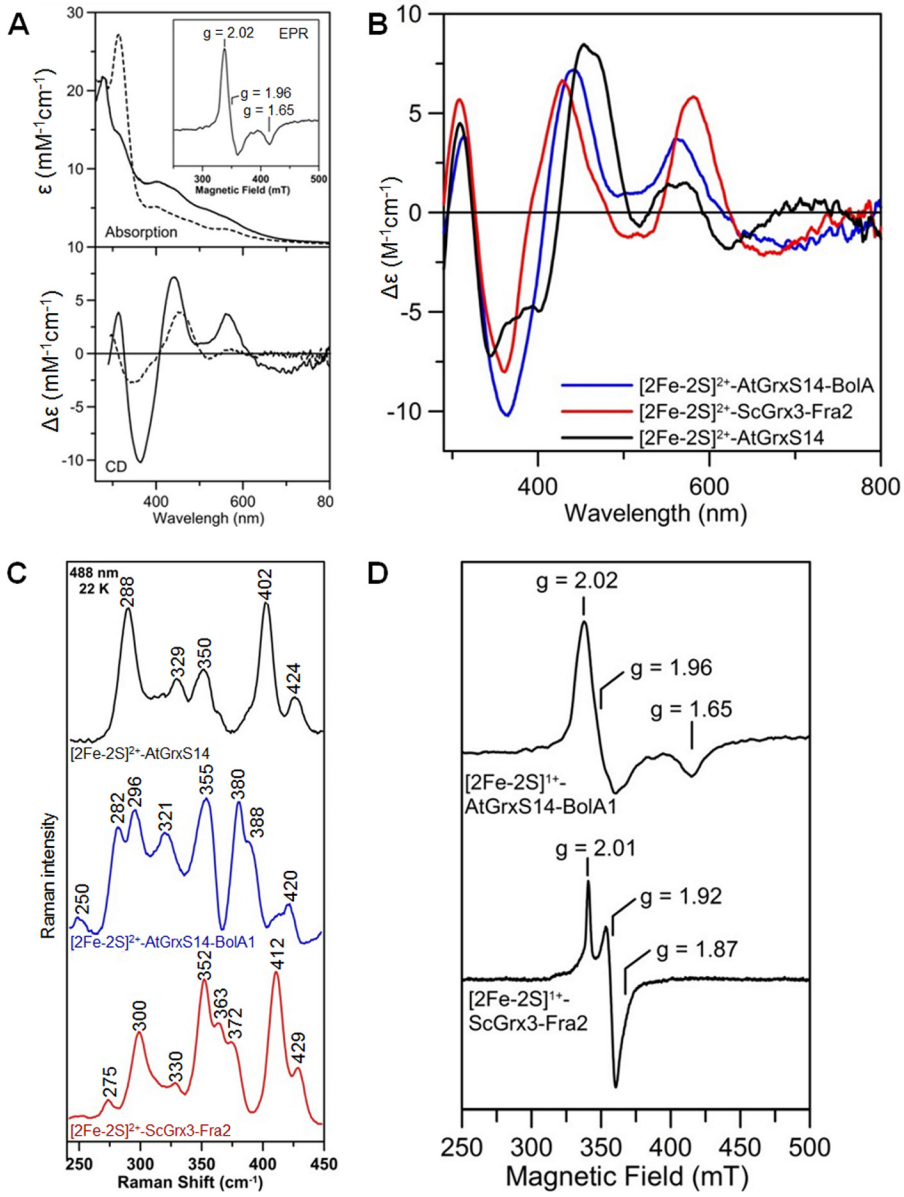

FIGURE 5. **Spectroscopic studies of AtGrxS14-BolA1 holo-heterodimers.** *A*, UV-visible absorption and CD spectra of oxidized (*solid line*) and dithionite-reduced (*broken line*) reconstituted AtGrxS14-BolA1 complex. ϵ and $\Delta\epsilon$ values are expressed per AtGrxS14-BolA1 heterodimer, and the intense band at 314 nm in the reduced absorption spectrum arises from excess dithionite. The *inset* shows the X-band EPR spectrum of the dithionite-reduced sample recorded at 10 K and 9.581 GHz, with a microwave power of 5 milliwatts and a modulation amplitude of 0.65 millitesla. *B*, comparison of the CD spectra of the $[2Fe\text{-}2S]^{2+}$ centers in the AtGrxS14-BolA1 and ScGrx3-Fra2 heterodimers and the AtGrxS14 homodimer. $\Delta\epsilon$ values are expressed per $[2Fe\text{-}2S]^{2+}$ cluster. *C*, comparison of the resonance Raman spectra of the $[2Fe\text{-}2S]^{2+}$ centers in the AtGrxS14-BolA1 and ScGrx3-Fra2 heterodimers and the AtGrxS14 homodimer. Spectra were recorded using 488-nm laser excitation. Samples were ~2 mM in the [2Fe-2S] cluster and were in the form of a frozen droplet at 17–22 K. Each spectrum is the sum of 100 scans, with each scan involving photon counting for 1 s at 0.5 cm^{-1} increments with 6 cm^{-1} spectral resolution. Bands due to lattice modes of ice have been subtracted from all spectra. *D*, comparison of the X-band EPR spectra of the dithionite-reduced $[2Fe\text{-}2S]^{1+}$ centers in the AtGrxS14-BolA1 and ScGrx3-Fra2 heterodimers. EPR conditions: microwave frequency, 9.581 GHz; modulation amplitude, 0.65 millitesla; microwave power, 5 milliwatts; temperature, 10 K. Spin quantification of both EPR signals indicates 1.0 ± 0.1 spins per [2Fe-2S] cluster.

Biological Function of Grx-BolA Apo- and Holo-heterodimers—An important question is how apo- and holo-Grx-BolA complexes are formed in the cells, as Grxs and BolAs are first translated as apoproteins and they might preferentially form apo-heterodimers. Hence, the Fe-S cluster might eventually be inserted through the functioning of the assembly machinery of the same compartment (*pathway 1* in Fig. 6*B*) (49). Consistently, a Grx-BolA apo-heterodimer can accept a [2Fe-2S] cluster from IscA, an A-type cluster donor (50). Interestingly, the NMR-based docking AtGrxS14-BolA2 apo-heterodimer model shows that the residues used for Fe-S cluster coordination from both partners are relatively well exposed and not directly implicated in the contact region.

Based on the observation that adding Fra2 to the more labile holo-homodimeric Grxs displaces the equilibrium toward the formation of a more stable ScGrx3-Fra2 holo-heterodimer (7), an alternative pathway to form Grx-BolA holo-heterodimers is from holo-homodimeric Grxs (*pathway 2* in Fig. 6*B*). Hence, there may be a dynamic equilibrium that is dependent on the expression and/or subcellular local-

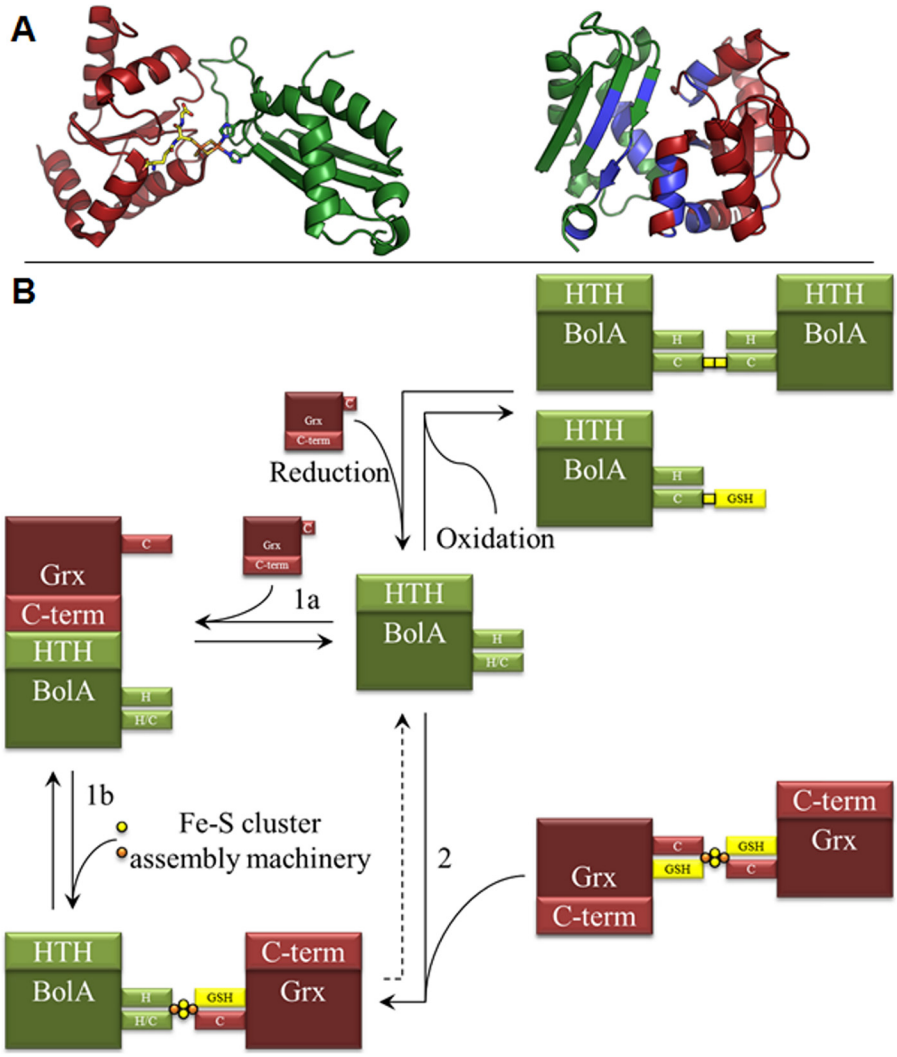

FIGURE 6. **Formation of BolA-Grx complexes.** *A*, comparison of AtGrxS14-BolA apo- and holo-heterodimers. The [2Fe-2S]-bridged AtGrxS14-BolA1 holo-heterodimer model was built from the structures of individual proteins. The model of AtGrxS14-BolA2 apo-heterodimer was obtained by NMR-based docking from residues (colored in *blue*) presenting high chemical shift variations upon partner addition. Grxs are colored in *green*, BolA are in *red*, and glutathione is in *yellow*. *B*, recapitulative scheme showing the formation of BolA-BolA and Grx-BolA complexes. From the current literature, there are two pathways to form Grx-BolA holo-heterodimers. Grx-BolA apo-heterodimers can accept a [2Fe-2S] cluster from IscAs or possibly other Fe-S assembly components (*pathway 1*) (50). Alternatively BolA can displace a Grx monomer from holo-homodimeric Grxs as shown for the ScGrx3-Fra2 couple (*pathway 2*) (7). In principle, the reactions are reversible, and monomeric BolAs or Grx-BolA apo-heterodimers could be reformed by disruption (7) of the Grx-BolA holo-heterodimer Fe-S cluster or its transfer to an acceptor. Due to the presence of a cysteine residue, BolA_Cs can form disulfide bridges either as covalent dimers or as glutathionylated forms, both forms being reversibly reduced by Grxs (10). The physiological relevance of each form has not been always elucidated, but interconversion can affect all assumed functions of both proteins (DNA binding, iron-sensing, or Fe-S cluster maturation).

ization of both proteins or on the presence of Fe-S cluster maturation or repair systems.

The function of these holo-heterodimers is still not clear (6, 9, 50, 51). The only characterized physiological role for a Grx-BolA holo-heterodimer is in sensing the intracellular iron/Fe-S cluster status in yeast. The current model is that a complex formed by Fra1, Fra2, Grx3, and Grx4 links the mitochondrial Fe-S or iron status to the control of a set of genes involved in iron uptake, transport, and storage known as the iron regulon via the regulation of Aft1 transcription factor (5). Under iron-deficient conditions, Aft1 is concentrated in the nucleus and activates the iron regulon, whereas under iron-sufficient conditions it is found predominantly in the cytoplasm. The current view is that Aft1 continuously shuttles between the cytosol and the nucleus but that specific signals maintain it in a given compartment. For instance, it was shown that its translocation from the nucleus to the cytoplasm is promoted by an iron-dependent multimerization and that Grx3/4 are essential for the nuclear export of Aft1 upon-iron replete conditions (52, 53). Importantly, the recognition of Aft1 involves at least a negatively charged region in the yeast Grx4 formed by the last 16 C-terminal residues (supplemental Fig. S2) (40). Overall, although it is not clear where the Grx-BolA complex is acting, it is very likely that the formation of the Fe-S cluster in the Grx-BolA heterodimer is crucial for Aft1 regulation. Indeed, the known Fe-S cluster ligands (GSH, Grx catalytic cysteine, and BolA invariant histidine) are all required for iron-dependent inhibition of Aft1 activity *in vivo* (8, 54). Accordingly, it was shown recently that a ScGrx3/4-Fra2 holo-heterodimer, but not Grx3 holo-homodimer, can transfer an Fe-S cluster to Aft2, used as an Aft representative, inducing Aft2 dimerization (6).

Although the mode of action and regulation of Aft1 is not yet completely elucidated, the formation of two types of Grx-BolA heterodimers involving different protein regions allows implementing the working model of Aft1 regulation. First, the observation that the Grx C-terminal region is accessible in holo-heterodimers suggests that in yeast cells under iron-replete conditions, the formation of Grx-BolA holo-heterodimers may contribute to the cytoplasmic retention/nuclear export of Aft1 either by simply recruiting it or by transferring their Fe-S clusters. On the contrary, in iron-depleted conditions, Grx and BolA should form apo-heterodimers. In this case the C-terminal tail of Grx is hidden by its partner, which should prevent the possibility of interacting with Aft1, allowing it to accumulate in the nucleus and to activate the genes placed under its control. The existence of these different types of complexes may explain why ScGrx3/4-Fra2 interactions were detected in cells independently of the iron status. Despite the fact that Aft1 is restricted to a few species, similar iron regulation systems might exist in other organisms including plants. For instance, in *Schizosaccharomyces pombe*, Fep1 and Php4, two transcriptional regulators of iron homeostasis, are regulated by a Grx4 ortholog (55, 56). Whether a BolA is required in this case is not yet elucidated.

In summary, in the case of the Grx-BolA holo-heterodimer, the interface comprises the conserved residue of the [H/C] loop and the invariant histidine of BolAs, a glutathione, and the catalytic cysteine of Grxs. Conversely, in the case of the Grx-BolA apo-heterodimer, the interaction surface between the two partners surprisingly includes the putative DNA binding anchor point of BolAs and the transcription factor binding surface of monothiol Grxs. Therefore, BolA and Grx function/activity can be adjusted via several post-translational events as all BolA types can form apo and holo-heterodimers with monothiol Grxs. Such an example where two proteins interact with two distinct regions is quite unusual.

Acknowledgments—Access to the Bruker DRX 600 (NMR) and x-ray diffraction facilities of the Université de Lorraine was appreciated. We are grateful to the staff members of Proxima-1 beamline of the SOLEIL Synchrotron and of BM30A beamline at European Synchrotron Radiation Facility.

REFERENCES

1. Nooren, I. M., and Thornton, J. M. (2003) Diversity of protein-protein interactions. *EMBO J.* **22,** 3486–3492
2. Aldea, M., Hernández-Chico, C., de la Campa, A. G., Kushner, S. R., and Vicente, M. (1988) Identification, cloning, and expression of bolA, an ftsZ-dependent morphogene of *Escherichia coli*. *J. Bacteriol.* **170,** 5169–5176
3. Santos, J. M., Freire, P., Vicente, M., and Arraiano, C. M. (1999) The stationary-phase morphogene bolA from *Escherichia coli* is induced by stress during early stages of growth. *Mol. Microbiol.* **32,** 789–798
4. Rouhier, N., Couturier, J., Johnson, M. K., and Jacquot, J. P. (2010) Glutaredoxins: roles in iron homeostasis. *Trends Biochem. Sci.* **35,** 43–52
5. Kumánovics, A., Chen, O. S., Li, L., Bagley, D., Adkins, E. M., Lin, H., Dingra, N. N., Outten, C. E., Keller, G., Winge, D., Ward, D. M., and Kaplan, J. (2008) Identification of FRA1 and FRA2 as genes involved in regulating the yeast iron regulon in response to decreased mitochondrial iron-sulfur cluster synthesis. *J. Biol. Chem.* **283,** 10276–10286
6. Poor, C. B., Wegner, S. V., Li, H., Dlouhy, A. C., Schuermann, J. P., Sanishvili, R., Hinshaw, J. R., Riggs-Gelasco, P. J., Outten, C. E., and He, C. (2014) Molecular mechanism and structure of the *Saccharomyces cerevisiae* iron regulator Aft2. *Proc. Natl. Acad. Sci. U.S.A.* **111,** 4043–4048
7. Li, H., Mapolelo, D. T., Dingra, N. N., Naik, S. G., Lees, N. S., Hoffman, B. M., Riggs-Gelasco, P. J., Huynh, B. H., Johnson, M. K., and Outten, C. E. (2009) The yeast iron regulatory proteins Grx3/4 and Fra2 form heterodimeric complexes containing a [2Fe-2S] cluster with cysteinyl and histidyl ligation. *Biochemistry* **48,** 9569–9581
8. Li, H., Mapolelo, D. T, Dingra, N. N., Keller, G., Riggs-Gelasco, P. J., Winge, D. R., Johnson, M. K., and Outten, C. E. (2011) Histidine 103 in Fra2 is an iron-sulfur cluster ligand in the [2Fe-2S] Fra2-Grx3 complex and is required for *in vivo* iron signaling in yeast. *J. Biol. Chem.* **286,** 867–876
9. Yeung, N., Gold, B., Liu, N. L., Prathapam, R., Sterling, H. J., Willams, E. R., and Butland, G. (2011) The *E. coli* monothiol glutaredoxin GrxD forms homodimeric and heterodimeric FeS cluster-containing complexes. *Biochemistry* **50,** 8957–8969
10. Couturier, J., Wu, H. C., Dhalleine, T., Pégeot, H., Sudre, D., Gualberto, J. M., Jacquot, J. P., Gaymard, F., Vignols, F., and Rouhier, N. (2014) Monothiol glutaredoxin-BolA interactions: redox control of *Arabidopsis thaliana* BolA2 and SufE1. *Mol. Plant* **7,** 187–205
11. Willems, P., Wanschers, B. F., Esseling, J., Szklarczyk, R., Kudla, U., Duarte, I., Forkink, M., Nooteboom, M., Swarts, H., Gloerich, J., Nijtmans, L., Koopman, W., and Huynen, M. A. (2013) BOLA1 is an aerobic protein that prevents mitochondrial morphology changes induced by glutathione depletion. *Antioxid. Redox Signal.* **18,** 129–138
12. Bandyopadhyay, S., Gama, F., Molina-Navarro, M. M., Gualberto, J. M., Claxton, R., Naik, S. G., Huynh, B. H., Herrero, E., Jacquot, J. P., Johnson, M. K., and Rouhier, N. (2008) Chloroplast monothiol glutaredoxins as scaffold proteins for the assembly and delivery of [2Fe-2S] clusters. *EMBO J.* **27,** 1122–1133
13. Brown, R. E., Jarvis, K. L., and Hyland, K. J. (1989) Protein measurement using bicinchoninic acid: elimination of interfering substances. *Anal. Biochem.* **180,** 136–139
14. Fish, W. (1988) Rapid colorimetric micromethod for the quantitation of complexed iron in biological samples. *Methods Enzymol.* **158,** 357–364
15. Kabsch, W. (2010) *XDS*. *Acta Crystallogr. D Biol. Crystallogr.* **66,** 125–132
16. Evans, P. (2006) Scaling and assessment of data quality. *Acta Crystallogr. D. Biol. Crystallogr.* **62,** 72–82
17. Winn, M. D., Ballard, C. C., Cowtan, K. D., Dodson, E. J., Emsley, P., Evans, P. R., Keegan, R. M., Krissinel, E. B., Leslie, A. G., McCoy, A., McNicholas, S. J., Murshudov, G. N., Pannu, N. S., Potterton, E. A., Powell, H. R., Read, R. J., Vagin, A., and Wilson, K. S. (2011) Overview of the CCP4 suite and current developments. *Acta Crystallogr. D. Biol. Crystallogr.* **67,** 235–242
18. Vagin, A., and Teplyakov, A. (2010) Molecular replacement with MOLREP. *Acta Crystallogr. D. Biol. Crystallogr.* **66,** 22–25
19. Adams, P. D., Afonine, P. V., Bunkóczi, G., Chen, V. B., Davis, I. W., Echols, N., Headd, J. J., Hung, L. W., Kapral, G. J., Grosse-Kunstleve, R. W., McCoy, A. J., Moriarty, N. W., Oeffner, R., Read, R. J., Richardson, D. C., Richardson, J. S., Terwilliger, T. C., and Zwart, P. H. (2010) PHENIX: a comprehensive Python-based system for macromolecular structure solution. *Acta Crystallogr. D. Biol. Crystallogr.* **66,** 213–221
20. Emsley, P., Lohkamp, B., Scott, W. G., and Cowtan, K. (2010) Features and development of Coot. *Acta Crystallogr. D. Biol. Crystallogr.* **66,** 486–501
21. Chen, V. B., Arendall, W. B., 3rd, Headd, J. J., Keedy, D. A., Immormino, R. M., Kapral, G. J., Murray, L. W., Richardson, J. S., and Richardson, D. C. (2010) MolProbity: all-atom structure validation for macromolecular crystallography. *Acta Crystallogr. D. Biol. Crystallogr.* **66,** 12–21
22. Delaglio, F., Grzesiek, S., Vuister, G. W., Zhu, G., Pfeifer, J., and Bax, A. (1995) NMRPipe: a multidimensional spectral processing system based on UNIX pipes. *J. Biomol. NMR* **6,** 277–293
23. Johnson, B. A., and Blevins, R. A. (1994) NMR view: a computer program for the visualization and analysis of NMR data. *J. Biomol. NMR* **4,** 603–614
24. Cheung, M. S., Maguire, M. L., Stevens, T. J., and Broadhurst, R. W. (2010) DANGLE: a bayesian inferential method for predicting protein backbone dihedral angles and secondary structure. *J. Magn. Reson.* **202,** 223–233
25. Vranken, W. F., Boucher, W., Stevens, T. J., Fogh, R. H., Pajon, A., Llinas, M., Ulrich, E. L., Markley, J. L., Ionides, J., and Laue, E. D. (2005) The CCPN data model for NMR spectroscopy: development of a software

pipeline. *Proteins* **59,** 687–696
26. Linge, J. P., O'Donoghue, S. I., and Nilges, M. (2001) Automated assignment of ambiguous nuclear overhauser effects with ARIA. *Methods Enzymol.* **339,** 71–90
27. Brünger, A. T., Adams, P. D., Clore, G. M., DeLano, W. L., Gros, P., Grosse-Kunstleve, R. W., Jiang, J. S., Kuszewski, J., Nilges, M., Pannu, N. S., Read, R. J., Rice, L. M., Simonson, T., and Warren, G. L. (1998) Crystallography & NMR system: a new software suite for macromolecular structure determination. *Acta Crystallogr. D Biol. Crystallogr.* **54,** 905–921
28. Tovchigrechko, A., and Vakser, I. (2006) GRAMM-X public web server for protein-protein docking. *Nucleic Acids Res.* **34,** W310–W314
29. Krieger, E., Joo, K., Lee, J., Lee, J., Raman, S., Thompson, J., Tyka, M., Baker, D., and Karplus, K. (2009) Improving physical realism, stereochemistry, and side-chain accuracy in homology modeling: four approaches that performed well in CASP8. *Proteins* **77,** 114–122
30. Keller, S., Vargas, C., Zhao, H., Piszczek, G., Brautigam, C. A., and Schuck, P. (2012) High-precision isothermal titration calorimetry with automated peak-shape analysis. *Anal. Chem.* **84,** 5066–5073
31. Katoh, K., and Standley, D. (2013) MAFFT multiple sequence alignment software version 7: improvements in performance and usability. *Mol. Biol. Evol.* **30,** 772–780
32. Gille, C., and Frömmel, C. (2001) STRAP: editor for STRuctural Alignments of Proteins. *Bioinformatics* **17,** 377–378
33. Kasai, T., Inoue, M., Koshiba, S., Yabuki, T., Aoki, M., Nunokawa, E., Seki, E., Matsuda, T., Matsuda, N., Tomo, Y., Shirouzu, M., Terada, T., Obayashi, N., Hamana, H., Shinya, N., Tatsuguchi, A., Yasuda, S., Yoshida, M., Hirota, H., Matsuo, Y., Tani, K., Suzuki, H., Arakawa, T., Carninci, P., Kawai, J., Hayashizaki, Y., Kigawa, T., and Yokoyama, S. (2004) Solution structure of a BolA-like protein from *Mus musculus*. *Protein Sci.* **13,** 545–548
34. Cheng, Z., Miura, K., Popov, V. L., Kumagai, Y., and Rikihisa, Y. (2011) Insights into the CtrA regulon in development of stress resistance in obligatory intracellular pathogen *Ehrlichia chaffeensis*. *Mol. Microbiol.* **82,** 1217–1234
35. Freire, P., Moreira, R. N., and Arraiano, C. M. (2009) BolA inhibits cell elongation and regulates MreB expression levels. *J. Mol. Biol.* **385,** 1345–1351
36. Shukla, M., Minda, R., Singh, H., Tirumani, S., Chary, K., and Rao, B. (2012) UVI31+ is a DNA endonuclease that dynamically localizes to chloroplast pyrenoids in *C. reinhardtii*. *PLoS ONE* **7,** 1–13
37. Valverde, R., Edwards, L., and Regan, L. (2008) Structure and function of KH domains. *FEBS J.* **275,** 2712–2726
38. Li, L., Cheng, N., Hirschi, K. D., and Wang, X. (2010) Structure of *Arabidopsis* chloroplastic monothiol glutaredoxin AtGRXcp. *Acta Crystallogr. D. Biol. Crystallogr.* **66,** 725–732
39. Li, H., Mapolelo, D. T., Randeniya, S., Johnson, M. K., and Outten, C. E. (2012) Human glutaredoxin 3 forms [2Fe-2S]-bridged complexes with human BolA2. *Biochemistry* **51,** 1687–1696
40. Hoffmann, B., Uzarska, M. A., Berndt, C., Godoy, J. R., Haunhorst, P., Lillig, C. H., Lill, R., and Mühlenhoff, U. (2011) The multidomain thioredoxin-monothiol glutaredoxins represent a distinct functional group. *Antioxid. Redox Signal.* **15,** 19–30
41. Li, S., Gutsche, N., and Zachgo, S. (2011) The ROXY1 C-terminal L**LL motif is essential for the interaction with TGA transcription factors. *Plant Physiol.* **157,** 2056–2068
42. Rotsaert, F. J., Pikus, J. D., Fox, B. G., Markley, J. L., and Sanders-Loehr, J. (2003) N-isotope effects on the Raman spectra of Fe(2)S(2) ferredoxin and Rieske ferredoxin: evidence for structural rigidity of metal sites. *J. Biol. Inorg. Chem.* **8,** 318–326
43. Kounosu, A., Li, Z., Cosper, N. J., Shokes, J. E., Scott, R. A., Imai, T., Urushiyama, A., and Iwasaki, T. (2004) Engineering a three-cysteine, one-histidine ligand environment into a new hyperthermophilic archaeal Rieske-type [2Fe-2S] ferredoxin from *Sulfolobus solfataricus*. *J. Biol. Chem.* **279,** 12519–12528
44. Iwasaki, T., Kounosu, A., Kolling, D. R., Crofts, A. R., Dikanov, S. A., Jin, A., Imai, T., and Urushiyama, A. (2004) Characterization of the pH-dependent resonance Raman transitions of archaeal and bacterial Rieske [2Fe-2S] proteins. *J. Am. Chem. Soc.* **126,** 4788–4789
45. Tirrell, T. F., Paddock, M. L., Conlan, A. R., Smoll, E. J., Jr., Nechushtai, R., Jennings, P. A., and Kim, J. E. (2009) Resonance Raman studies of the (His)(Cys)3 2Fe-2S cluster of MitoNEET: comparison to the (Cys)4 mutant and implications of the effects of pH on the labile metal center. *Biochemistry* **48,** 4747–4752
46. Bertrand, P., Guigliarelli, B., Gayda, J., Peter, B., and Gibson, J. (1985) A ligand-field model to describe a new class of 2Fe-2S clusters in proteins and their synthetic analogues. *Biochim. Biophys. Acta* **831,** 261–266
47. Guigliarelli, B., and Bertrand, P. (1999) Application of EPR spectroscopy to the structural and functional study of iron-sulfur proteins. *Adv. Inorg. Chem.* **47,** 421–497
48. Link, T. (1999) The structures of Rieske and Rieske-type proteins. *Adv. Inorg. Chem.* **47,** 83–157
49. Couturier, J., Touraine, B., Briat, J. F., Gaymard, F., and Rouhier, N. (2013) The iron-sulfur cluster assembly machineries in plants: current knowledge and open questions. *Front Plant Sci.* **4,** 259
50. Mapolelo, D. T., Zhang, B., Randeniya, S., Albetel, A. N., Li, H., Couturier, J., Outten, C. E., Rouhier, N., and Johnson, M. K. (2013) Monothiol glutaredoxins and A-type proteins: partners in Fe-S cluster trafficking. *Dalton Trans.* **42,** 3107–3115
51. Cameron, J. M., Janer, A., Levandovskiy, V., Mackay, N., Rouault, T. A., Tong, W. H., Ogilvie, I., Shoubridge, E. A., and Robinson, B. H. (2011) Mutations in iron-sulfur cluster scaffold genes NFU1 and BOLA3 cause a fatal deficiency of multiple respiratory chain and 2-oxoacid dehydrogenase enzymes. *Am. J. Hum. Genet.* **89,** 486–495
52. Pujol-Carrion, N., Belli, G., Herrero, E., Nogues, A., and de la Torre-Ruiz, M. (2006) Glutaredoxins Grx3 and Grx4 regulate nuclear localisation of Aft1 and the oxidative stress response in *Saccharomyces cerevisiae*. *J. Cell Sci.* **119,** 4554–4564
53. Mühlenhoff, U., Molik, S., Godoy, J. R., Uzarska, M. A., Richter, N., Seubert, A., Zhang, Y., Stubbe, J., Pierrel, F., Herrero, E., Lillig, C. H., and Lill, R. (2010) Cytosolic monothiol glutaredoxins function in intracellular iron sensing and trafficking via their bound iron-sulfur cluster. *Cell Metab.* **12,** 373–385
54. Ojeda, L., Keller, G., Muhlenhoff, U., Rutherford, J. C., Lill, R., and Winge, D. R. (2006) Role of glutaredoxin-3 and glutaredoxin-4 in the iron regulation of the Aft1 transcriptional activator in *Saccharomyces cerevisiae*. *J. Biol. Chem.* **281,** 17661–17669
55. Jbel, M., Mercier, A., and Labbé, S. (2011) Grx4 monothiol glutaredoxin is required for iron limitation-dependent inhibition of Fep1. *Eukaryot Cell* **10,** 629–645
56. Mercier, A., and Labbé, S. (2009) Both Php4 function and subcellular localization are regulated by iron via a multistep mechanism involving the glutaredoxin Grx4 and the exportin Crm1. *J. Biol. Chem.* **284,** 20249–20262
57. Baker, N. A., Sept, D., Joseph, S., Holst, M. J., and McCammon, J. A. (2001) Electrostatics of nanosystems: application to microtubules and the ribosome. *Proc. Natl. Acad. Sci. U.S.A.* **98,** 10037–10041
58. Johansson, C., Roos, A. K., Montano, S. J., Sengupta, R., Filippakopoulos, P., Guo, K., von Delft, F., Holmgren, A., Oppermann, U., and Kavanagh, K. L. (2011) The crystal structure of human GLRX5: iron-sulfur cluster co-ordination, tetrameric assembly and monomer activity. *Biochem. J.* **433,** 303–311